IEEE Access
Multidisciplinary ⋮ Rapid Review ⋮ Open Access Journal

Received 29 September 2022, accepted 18 October 2022, date of publication 21 October 2022, date of current version 27 October 2022.

Digital Object Identifier 10.1109/ACCESS.2022.3216373

RESEARCH ARTICLE

Cross-Shaped Interconnected Receiver–Transmitter Metasurface for a Circularly Polarized Fabry–Pérot Antenna

QIANG CHEN[1], XIONG ZOU[1], LIANG HONG[1], DI ZHANG[1], SIYU HUANG[1], FANGLI YU[1], WEIHUA XIONG[1], AND HOU ZHANG[2]

[1]Air Force Early Warning Academy, Wuhan, Hubei 430019, China
[2]Air and Missile Defense College, Air force Engineering University, Xi'an, Shaanxi 710051, China

Corresponding author: Qiang Chen (1062620145@qq.com)

This work was supported by the National Natural Science Foundation of China under Grant 62101592.

ABSTRACT In this paper, we proposed a cross-shaped interconnected receiver–transmitter (RT) metasurface (MS) that was employed for a high-aperture-efficiency, high-gain, circularly polarized Fabry–Pérot (FP) antenna. The RT-MS unit cell consists of upper-layer cross-shaped patch and lower-layer squared patch that are connected by two metal-probes that cross the sandwiched middle metal-plane. The bottom patch receives electromagnetic wave, functioning as receiver, and transfers it to the top cross-shaped patch passing through the two mental probes. Through tuning the relative locations of the two probes, equal amplitude and 90° phase difference can be obtained, thereby achieving linear to circular polarization conversion performance, indicating that the MS has the ability of tuning transmission coefficients independently. Meanwhile, the MS is designed to present high reflectivity that high-gain property is obtained when forming a FP cavity. Then, an off-center coaxial patch antenna is applied as feeder due to its stable radiation performance. To further enhance the performance of the source antenna, an AMC structure is adopted to improving the radiation gain, efficiency and radiation directivity by suppressing surface wave loss. Meanwhile, the profile was also reduced. The linearly polarized wave emitting from the feeder multi-reflected in the FP cavity formed by MS superstrate and AMC structure, and then transmit it in phase to the space, thus a high-gain and CP radiation is achieved as final. The measurements demonstrate that the proposed RT-MS-based antenna perform a maximum gain of 18.7dBic at 9.4GHz with aperture efficiency of 76.7%, and a circular polarization bandwidth within 9.2-9.7GHz, while, the antenna owns a compact size of only $2.85\lambda_0 \times 2.85\lambda_0$. Thus, a novel RT-MS-based FP antenna exhibit a good radiation performance that can be a candidate in applying to communication and point-to-point links.

INDEX TERMS Cross-shaped, RT-MS, Fabry-Pérot (FP), polarization conversion, circular polarization, aperture efficiency.

I. INTRODUCTION

Circularly polarized (CP) antennas play an important role in wireless communication systems and point-to-point links owing to their high tolerance to multi-path effects and polarization mismatching, so there is a high demand for CP antennas with properties such as a high gain, wideband, and a wide 3-dB axial ratio angle. CP antennas are designed by many methods. Among them, metasurfaces have proved to be efficient in CP generation and performance enhancement. Thus, a series of linear-to-circular polarization conversion metasurface-based antennas have been designed [1], [2], [3], [4], [5], [6], [7], [8]. In previously reported MS-based antennas, slot source antennas were usually used as feeders for their wideband to produce linear polarized waves, which could be generated after passing through a polarization conversion metasurface (PCM), a polarization conversion to the CP mode [1], [2], [3], [4]. Owing to their high gain property, several

The associate editor coordinating the review of this manuscript and approving it for publication was Tutku Karacolak.

Fabry–Pérot (FP) resonant cavity antennas have been proposed in the design of circularly polarized antennas (CPAs) [9], [10], [11], [12], [13], [14], [15]. A PCM array consisting of two neighboring metal-coating-substrate unit cells, which act as a superstrate and feeding slot antenna, was combined in an FP-CP antenna [1], realizing an enhanced gain and wideband CP radiation while maintaining a compact size. Another FP resonant cavity was formed by an all-metal cross-slot-etched frequency-selective surface (FSS) and a nonstandard artificial magnetic conductor (AMC) [16]. Fed by an obliquely placed patch, the antenna achieved high gain, wideband CP performance [17]. Other polarization-reconfigurable MS-based FP-CPs was also reported [18]. However, the gain and bandwidth improvements were not enough due to a low reflectivity in FP resonance process that make it weakened greatly. In [1], that consists of a three-layer metal plane acting superstrate and a slot-coupled-fed antenna acting as a feeder achieves properties enhancement owing to effect by FP resonance, while the reflectivity of PCM was not taken account into the design. To realize preferable gain and wide band performance, array technique was applied in the design process in [7] and [17]. But at the same time it causes a larger size and a more complex feeding network that make it higher accuracy in fabrication. Hence, to make the bandwidth and gain enhancement to a maximum, a FP cavity should met two requirements: firstly, the appropriate gap separated by the PCM and the plane ground that make the transmitted wave being out to space in phase; and then having a high-reflectivity, which take the directivity higher. Thus, to obtain high-gain and nice CP radiation property, that reflection and transmission coefficients of the unit cell were controlled independently should be taken into the account into the PCM design. And the transmission coefficients determine the polarization conversion, and the resonance of the antenna depends on the reflection coefficient.

Following this, the receiver–transmitter metasurface (RT-MS) suggests a possible FP cavity antenna with high reflectivity and low transmissivity, resulting in high gain [22], [23]. RT-MS generally consists of receiver and transmitter patches, along with a coupling layer. The incident wave is received by the bottom patch and coupled with the top patch [24], [25]. An off-center metal via connecting receiver and transmitter was adapted to couple energy radiated by the slot antenna, resulting in a CP mode and achieving a high gain [21]. However, those reports mostly focus on the design of PCM, while paying little attention on how to enhance the radiation property of the source feeding antenna that can further improve radiation performance of those antennas better. Moreover, high aperture efficiency, while compact size simultaneously is the key to design a high-gain antenna, and thus it poses challenge to the design of RT-MS. Considering this, a cross-shaped interconnected RT-MS is proposed in this paper that can control reflection and transmit coefficients independently, and thus result in high reflectivity and polarization conversion through adjusting the size of the unit cell appropriately.

This design adopts a double-metal-probe connecting the square receiver and transmitter that is shaped by cross-like, which have high reflectivity and low transitivity and potentially increase the aperture efficiency further. Mean-while, the independent controlled capacity in reflection and transmission coefficients of the proposed RT-MS makes it a candidate in applying to high-gain, high apertue efficiency, and CP antennas. In the other hand, to further improve the radiation performance of the source antenna, 9×9 arranged periodically AMC structure is positioned surrounding the radiated patch. The FP resonance cavity is formed by the 9×9 unit cell array and AMC structure that is separated by the air gap with a certain distance. Simulations and measurement evidently demonstrates this design that the proposed antenna shows high-gain, high-aperture efficiency, and wideband CP characteristics that can be apply in many areas for high performance communication.

The remainder of this article is organized as follows. Section II provides the design procedure and analysis of the proposed RT-PCM with high reflectivity and circular polarization conversion. Section III presents the design and analysis of the FP-CP antenna. Section IV validates the design by simulated and measured results. We provide our conclusions in section V.

II. DESIGN PROCESS AND ANALYSIS OF PROPOSED PCM

Generally, in a PCM-based antenna, an FP cavity is formed by a PCM and ground plane separated by a certain distance. As shown in Fig. 1, the electromagnetic wave illuminated by the radiator in the center of the cavity can be multiply reflected and transmitted into space.

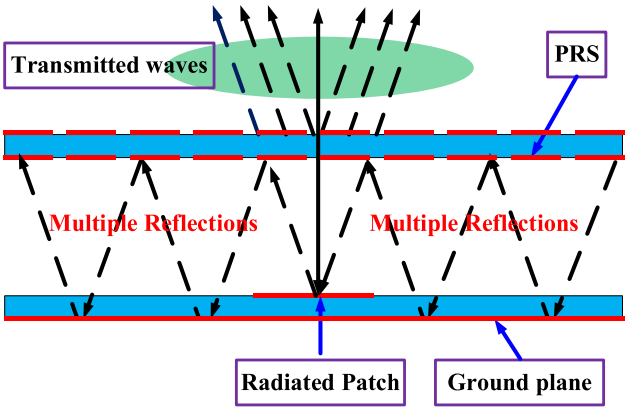

FIGURE 1. Ray theory model of the Fabry–Pérot cavity antenna for increasing directivity.

To obtain the maximum directivity, reflected and re-reflected waves in the cavity must be transmitted in phase. Hence, as shown in (1), the reflection phases of the ground plane, ϕ_{GND}, and those of PCM, ϕ_{PCM}, should satisfy

$$\phi_{\mathrm{pcm}} + \phi_{\mathrm{GND}} - \frac{4\pi h_c}{\lambda_0} = 2N\pi, \quad N = 0, \pm 1, \pm 2 \ldots. \tag{1}$$

Hence, a separation distance, h_c, between them can be determined. Once the feeding antenna is designed, the center frequency and ϕ_{GND} are basically fixed; that is, by optimizing ϕ_{PCM}, a relatively smaller resonance mode, N, can be selected, and a low profile can be obtained.

The boresight directivity of the antenna can be calculated as in [21]:

$$D_r = 10 \log \frac{1+R}{1-R}, \tag{2}$$

where R is the reflection magnitude of the PCM. Thus, a higher directivity is generated when R is larger, with the maximum directivity occurring when R is around 0.9 [27].

Based on the above analysis, when designing a CP-FP resonant antenna, three requirements should be met. The reflectivity of the proposed PCM must be high enough to achieve a high gain. The transmission coming from the cavity for coefficients T11 and T21 should have a phase difference of 90°, and be of equal or almost equal magnitude, to be transformed from LP to CP. Note that we define T11 as the transmission coefficient of the transfer of x-polarized waves to x-polarized waves when passing through PCM. So T21 represents the transfer of x-polarized waves to y-polarized waves when passing through PCM, where polarization conversion is realized. Then, as a source antenna feeding the PCM, the linear-polarized radiation should be high-gain enough, nice aperture efficiency, and wideband. Hence, we use the following design process.

As shown in Fig.2, we proposed a cross-shaped interconnected RT-MS that is composed by three-layer printed metal-coating and two neighboring identical substrates. The substrate is made of Rogers RT ($\varepsilon_r = 2.2$, $\tan\delta = 0.0014$) that is sized by 10 mm × 10 mm. The lower-layer patch is squared, while the upper-layer patch was cross-shaped-like designed, then, to excite a CP mode, two metal-probes connecting them that cross the sandwiched middle metal-plane were introduced in the design process. The two metal-probes were located at vertical and horizontal bars of the cross-shaped patch along x and y axis, respectively. The off-center distance was the same. Fig.2 (d) depicted the simulation model of the unit cell in HFSS that port 1 and port 2 were set along z axis positioned at a certain distance away from the unit cell, whereas the electric and magnetic wall boundary are set along x and y axis. The electromagnetic wave received by the receiver patch, and then passes through the two metal-probes to the transmitter patch. Due to having the capacity of amplitude and phase controlling in transmission coefficients, the unit cell radiates circularly polarized wave into the free space as final. In this design, the receiver patch is squared that make the unit cell achieve high reflectivity, then, according to the theoretical analysis, high-gain performance is obtained. Hence, having polarization conversion and high reflectivity characteristics simultaneously will be taken account to the design of the RT-MS.

Usually, a conventional RT-MS consisting of three-layers patches printed on both sides of the substrates can achieve high reflectivity through adjusting the length of the patches that obtain high-gain performance, then, to achieve circular polarization property, Ref. [21] proposed a corner cut transmitter RT element to generate CP mode through adjusting the off-center distance of the metal-via. As shown in Fig.2, the proposed RT-MS element adopts cross-shaped stubs interconnecting the receiver patch by two metal-probes. So, orthogonal components of E-fields can be generated that circular polarization radiation was produced.

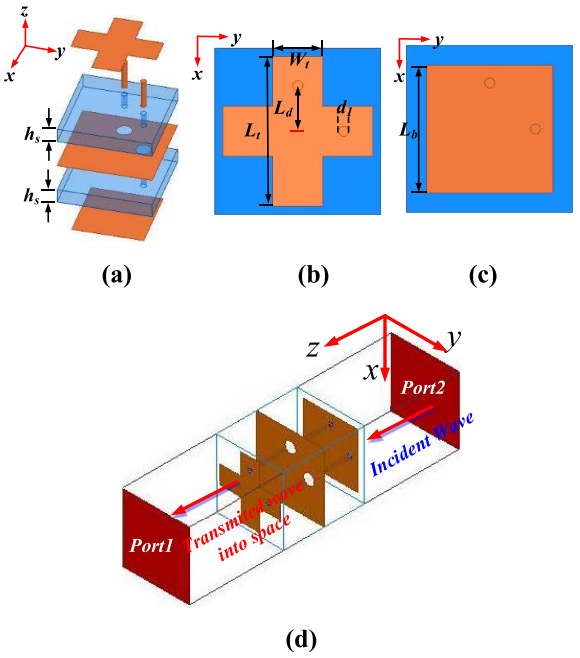

FIGURE 2. Configuration of the proposed RT-MS unit cell. Detail views of the unit cell: (a) Perspective view; (b) CP transmitter patch; (c) LP receiver patch; (d) simulated model of the unit cell in HFSS.

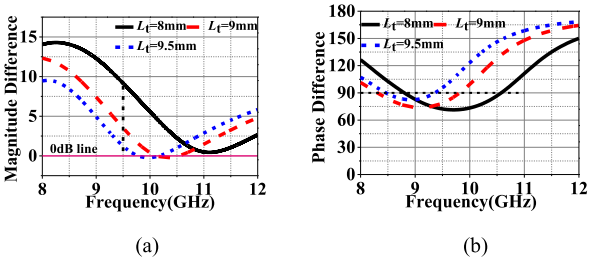

FIGURE 3. Effect of L_t on (a) Magnitude difference; (b) Phase difference.

As depicted in Fig.3, we investigate the transmission coefficients of the unit cell when the length of the cross-shaped stub, L_t, was varied. Then, it can be seen that the magnitude difference decreases as L_t increases from 8mm to 9.5mm, whereas little influence on the phase difference that remains about 90°. While, as shown in Fig. 4, another important parameter, the offsetting distance of the metal-probe, L_d, is also investigated that we can see that both magnitude and phase difference are affected by L_d. But, it's worth noting

that when L_d is more than 3mm, magnitude differences of the transmission coefficients are little affected whereas influencing on phase of that. When L_d is set to 3mm, an equal magnitude and 90° pahse difference was reached out that a CP mode is introduced. Above all, the magnitude and phase difference can be tuned independently that benefit for the design of the PCM.

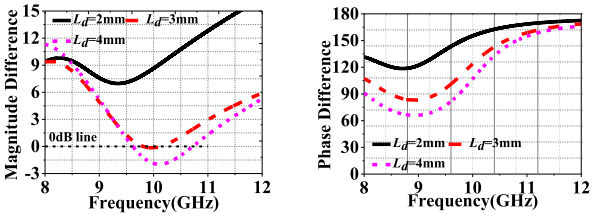

FIGURE 4. Effect of L_d on (a) Magnitude difference; (b) Phase difference.

As plot in Fig.5, the proposed RT-MS element achieves a high reflectivity magnitude of 0.81 at 9.5GHz that was dominated by co-polarization component, R_{xx}, whereas cross polarization one of that, R_{xx}, is very low that is close to zero, thus ensuring a high gain of the FP-CP antenna according to formula [21]. This indicates that the wave coming out of the cavity is almost x-polarized when illuming x-polarized wave, suggesting that the unit cell does not have the capability of polarization conversation for reflection wave. While, as shown in Fig.5 (b), an equal magnitude and 90° phase difference of transmission coefficients is occurred at 9.5GHz, which indicates that a CP mode is introduced. In addition, according the two prerequisites ensuring CP wave passing through PCM in Ref. [1], the unit cell achieves the LCPC band of 9.25-9.9GHz that performs a wide polarization conversion band.

Besides, the phase of T_{xx} is always ahead of that of T_{yx}, thus a RHCP wave towards z direction is radiated by RT-MS-based patch.

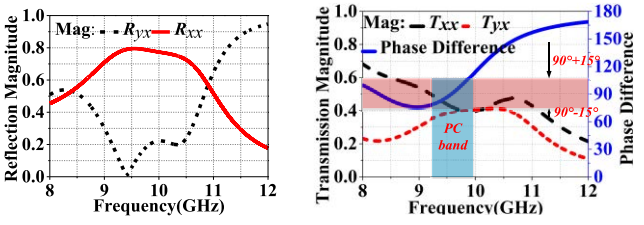

FIGURE 5. (a) S parameters of the unit cell and (b) Magnitudes and phases difference of transmission versus frequency for the optimum values granted to the unit cell.

Through above analysis, the CP mode that is produced by two prerequisites for equal magnitude and 90° phase difference is achieved at 9.5GHz. Then, to better illustrate how the cross-polarization component introduced clearly, we simulated the E-field distributions of the only one inner-connected metal-probe RT-MS.

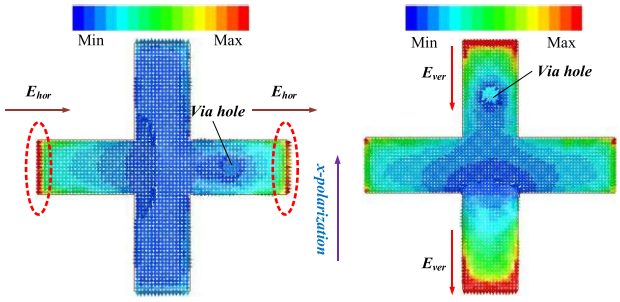

FIGURE 6. Simulated E-field distributions at 9.5 GHz illumining with vertical plane wave.

Assuming illuminated by a vertical plane wave, the electromagnetic wave couple passing through the only one inner-connected metal-probe locating at the horizontal strips of the cross-shaped patch to the radiated patch. Then, the E-field distributions are plot in Fig. 6 that it was more dominant on the edge of the horizontal strip, while much weaker on that of the vertical. Thus, it demonstrates that the horizontal-set metal-probe can excite a horizontal linearly-polarization mode. Meanwhile, similarly once the illuminati -on with the same vertical wave passing through the vertical -set inner-connected metal-probe, then the cross-shaped patch would achieve radiation with vertical linearly-polarization, as shown in Fig.6(b), and then we can see that the dominated E-field distributions also concentrate on the edge part of the vertical stubs. Following this, let us consider that take the two perpendicularly-set metal-probes together to the design and then illuminated by the linear-polarized wave, then according to above analysis, it would realize the horizontal and vertical-polarized E-fields, simultaneously. According to the superposition theorem, the total E-field can be written as:

$$E^t = E_0\hat{y} + E_0 e^{j\pi/2}\hat{x}, \tag{3}$$

and thus the circularly polarization is produced. Thereby, in this design, the two perpendicularly-set metal-probes inner-connecting cross-shaped RT-MS is adopt that a CP mode is easily achieved through adjusting the distance of the off-centered probe flexibly.

Moreover, to verify this design, the surface current distributions on the radiated patch of the unit cell at the phase angles of 0°, 90°, 180°, and 270° were plot in Fig. 7. As shown in Figs, the density currents were weak on both the horizontal and vertical stubs at the phase angle of 0° that were more dominant on the edge of the horizontal strip, while the density currents was much higher on both horizontal and vertical strip at the phase angle of 90°. Similar trends were occurred at the phase angle of 180° and 270°, respectively. Moreover, the direction of the current vector on the patch at 0° is opposite to that at 180°, that is to say, a 180° phase rotation of the currents is generated. And the same phenomenon was observed at 180° and 270°. In addition, the detailed vector

directions at four phase angles were marked in the figures, respectively. Then, it can come to a conclusion that a CP radiation is achieved by introducing 90° rotation after one quarter in the current distribution of the cross-shaped patch that a right-handed circularly polarized radiation is obtained by the designed MS.

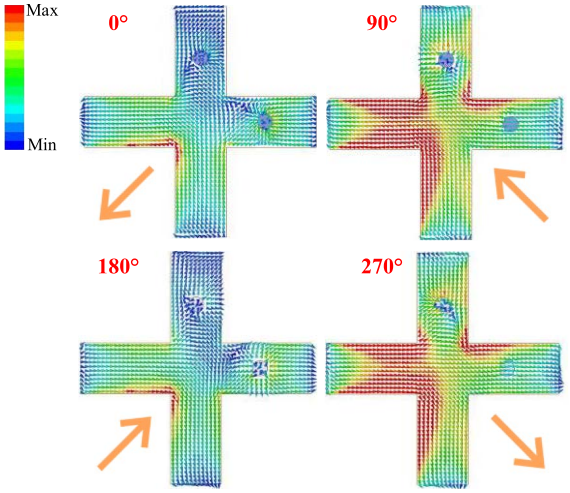

FIGURE 7. Simulated J-surf distributions at 9.5 GHz on the transmitter at the phase angles of 0°, 90°, 180°, and 270°.

III. ANALYSIS AND DESIGN OF PROPOSED CP-FP ANTENNA

The proposed antenna was created by the PCM superstrate and source antenna. Hence, the feeding source antenna having stable broadside radiation is required that a coaxial-type patch is unitized as feeder in this design, as shown in Fig.8 (b). The coaxial-type patch has non-uniform lengths in x and y direction, P_x and P_y, for impedance matching well. The coaxial-fed point is off-centered, and the distance to the center of the patch in x and y directions, namely S_x and S_y, is identical. The substrate is made of Rogers TMM4 ($\varepsilon_r = 4.4$, $\tan\delta = 0.0014$), with a thickness of 1 mm. The ground plane is squared and backed printing on the substrate. Thus, wide bandpass with lower than -10dB and stable radiation performance was achieved, as shown in Fig.8 (a) (b). To further enhance the radiation property, an AMC structure surrounding the patch is adopt. The AMC unit cell consists of a square metal patch with length of L_a, and is arranged periodically by 9×9 array except for allowing space for the radiated patch.

As plot in Fig.12, a 2.5dBic gain enhancement is achieved, and impedance matches better simultaneously when the AMC structure was loaded. As depicted in Fig.10, to clearly explain the enhancement principle, E-field vector and the operating modes sketches of the AMC-based feeder is given. As shown in Fig.11, only one resonance frequency point is produced by the only patch feeder though a very little variation of value of reflection coefficients occurring across 9.3 to 9.5GHz, while one more additional resonance, TM20, is generated by the introduction of the AMC. Thus, it comes to a conclusion that the wideband performance is gained by the fusion of the multiple order modes. Moreover, owing to the electromagnetic wave spearing across the whole AMC, then, the aperture efficiency will be accordingly increased. Meanwhile, the gain was enhanced due to the spearing out wave across the AMC unit cell that acts as radiated source additionally.

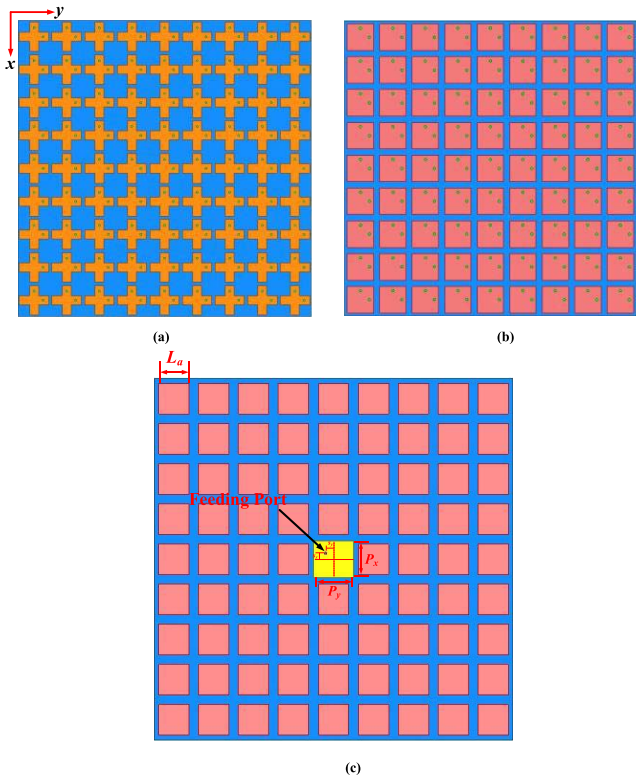

FIGURE 8. Configuration of the proposed FP-CP resonant antenna and detailed views: (a) Top view of the PCM; (b) Bottom view of the PCM; (c) AMC-loaded feeding antenna.

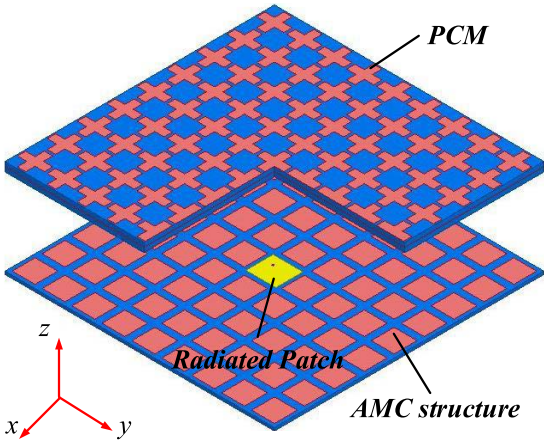

FIGURE 9. Configuration of proposed FP-CP antenna.

Then, to guarantee a satisfactory gain property, a larger size is preferred to avoid wave diffraction at the edge of the cavity.

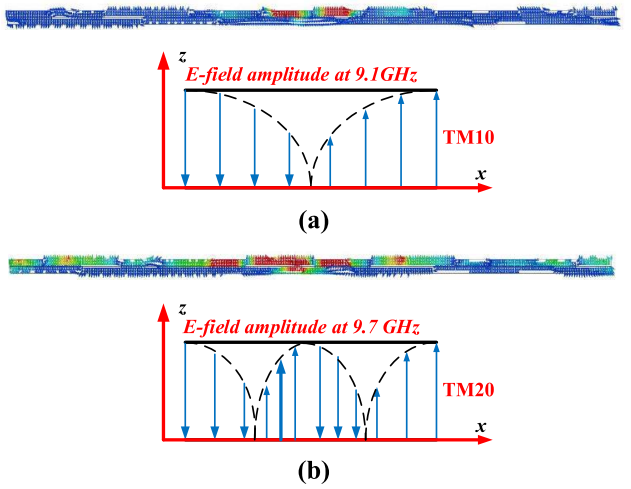

FIGURE 10. E-field vectors of the unit cell and the sketches of the operation modes at (a) 9.1GHz and (b) 9.7GHz.

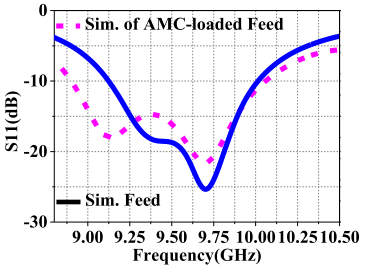

FIGURE 11. Simulated S parameters of the proposed FP-CP antenna with AMC-loaded feed and Feed.

TABLE 1. Optimal dimensions of proposed RT-MS.

Dimension	Size (mm)	Dimension	Size (mm)
h_s	1.524	L_a	7.6
W_t	2.75	P_x	9.1
L_d	2.75	P_y	10
L_t	9	S_x	1.5
L_b	8.1	S_y	2
d_1	0.8		

However, owing to the small contribution in gain enhancement on the edge of the MS and less energy distributed on the cavity edge as the size increases, the aperture efficiency, that is,

$$\eta = G\frac{\lambda_0^2}{4\pi A}, \tag{4}$$

decreases, where G is the boreside gain, and A is the physical size of the aperture. Through numerical simulations, a tradeoff is made between gain and efficiency. Consequently, a 90 mm × 90 mm PCM array with a 9 × 9-unit cell is formed, as shown in Fig. 8. (Table 1).

IV. SIMULATED AND MEASURED RESULTS

To validate the proposed RT-MS-based antenna, a prototype antenna is fabricated and measured. As shown in Fig.8, a simulated S11 bandwidth of 9-9.9GHz is achieved that agrees well with the measure results except for some reasonable error. The S11 of the feed and that of the AMC-based one was also plot in the figures, demonstrating that a more wideband and excellent impedance matching property is realized in this design, as shown in Fig.12 (a). The measured AR and the realized gain performance was plot in Fig.12 (b), which agree well with the simulated results. The measured AR has a bandwidth of 9.2-9.8GHz, and the minimum AR value is around 0.7dB occurred at the operated frequency, 9.5GHz. The proposed antenna achieves a flat realized gain higher than 18dBic within the impedance bandwidth, and the maximum one reaches 19.8dBic with a gain enhancement of 10dBic compared with the AMC-loaded feed, whereas whose gain is 2 dBic higher than that of feed, suggesting a better CP radiation. In addition, we also explore the AR performance versus angle that we can see in Fig.13 (a) that the AR value lower than 3dB cross the angles ranging from $-20°$ to $+18°$ in yoz plane, though having a little narrow in the xoz plane. Then, the aperture efficiency is also taken account to the evaluation of radiation property that Fig.13 (b) plots a maximum aperture efficiency of 89% occurred at 9.15GHz within the operated band. Meanwhile, in the whole operated band, the antenna own the aperture efficiencies of no lower than 60%, which presents a better radiation performance compared to other recent works, and the measured results agree well with that of the simulated though having about no more than 0.5% degeneration that can be tolerated reasonably.

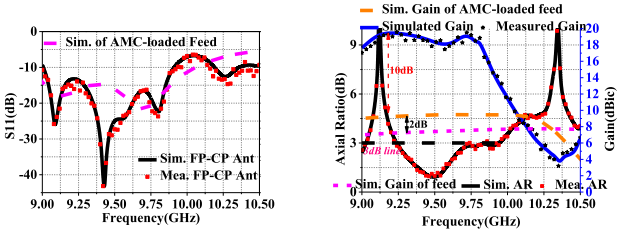

FIGURE 12. Comparisons of Simulation and mensuration of proposed CP-FP antenna with and without AMC-loaded (a) S11; (b) AR and bore-side gain.

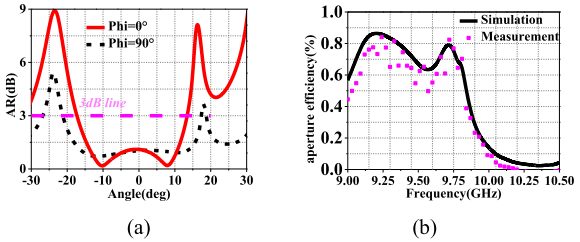

FIGURE 13. (a) simulated AR versus the angle in *xoz* plane and *yoz* plane; (b) Simulated and measured aperture efficiency of proposed CP-FP antenna.

In other hand, we also investigate another important parameter, the radiation pattern of the antenna, which depicted

TABLE 2. Performance comparison of the recently reported CP-FP antennas.

Ref.	Size (λ_0^3)	3 dB AR BW (GHz)	Peak gain (dBic)	Aperture Efficiency	3dB AR angle range	High-gain method	Operating bandwidth (GHz)
Proposed	**2.85 ×2.85×0.54**	**9.2-9.8**	**19.8**	**89%**	**-20° to 20°**	**FP Cavity and AMC**	**9-9.9**
[1]	2.0×2.0×0.45	8.1–10.0	11.2	25.6%		FP Cavity	8.25–9.5
[16]	2.20×2.20×0.8	2.51–2.56	13.3	-	-	FP Cavity	2.49–2.52
[17]	4.8×4.8×0.24	12.9–14.7	17.2	-	-	FP Cavity and array	12.95–13.95
[21]	3×3×0.19	9.7–10.3	17.8	53%	-15° to 15°	FP Cavity	9.8–10.2
[26]	2.0×2.0×0.6	7.3–7.6	15.1	42.3	-	FP Cavity	7.3–7.6
[27]	2.6×2.63×0.36	9.8–10.2	13.4	24.5%	-10° to 10°	FP Cavity	9.86–10.14
[28]	2.0×2.0×0.88	4.12–6.39	14.5	56.1%		FP Cavity	3.82–6.01

Note: "-" represents null.

the simulated and measured results in *xoz* plane and *yoz* plane at 9.5GHz, respectively, in Fig.14. Then, the antenna is demonstrated achieving a good radiation pattern with the cross-polarization levels less than −32dB and the side lobe levels less than −16dB whether in the E plane or H plane. In addition, the radiation pattern was measured that the main lobe is almost the same as that of the simulation, suggesting obtaining a better radiation performance once again.

To better present a better radiation property owned by the designed antenna, a comparison with recent related works is shown as list in Table 2 that the proposed RT-MS-based FP antenna is found to obtain a more higher gain and aperture efficiency in such a compact size with $2.8\lambda_0 \times 2.8\lambda_0$ and a achieved wider CP radiation through adopting a double meta-metal interconnecting the cross-shaped patch transmitter and receiver, thus CP mode introduced. Hence, the proposed antenna shows good radiation performances that demonstrate the correctness of this design.

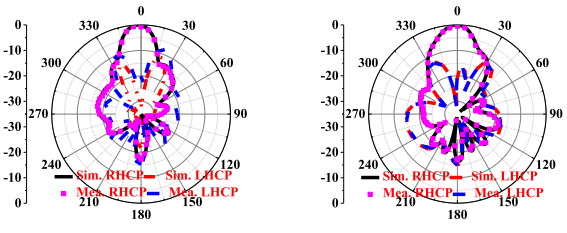

FIGURE 14. Simulated and measured radiation pattern at 12.5 GHz in (a) *xoz* plane and (b) *yoz* plane.

Besides, to achieve a LHCP wave, we just change the position of one of the two metal-probes to an opposite direction with the same off-center distance along x or y axis, as shown in Fig.15 (a), thus designing for the LHCP FP antenna. As shown in Fig.15 (b), the modified PCM is applied for the improved model, thus LHCP FP antenna was constructed. Then, through simulated, the results for the new antenna is exactly the same as those for the proposed antenna, except for the CP characteristic that indicate the design achieving both LHCP and RHCP wave just through a slight change.

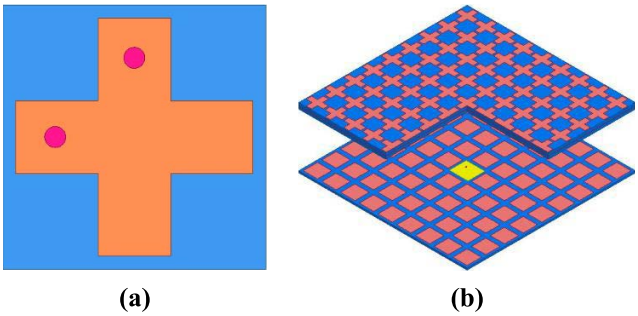

FIGURE 15. (a) the configuration of the LHCP unit cell; (b) 3D view of the geometry of the LHCP FP antenna.

V. CONCLUSION

In this paper, an interconnected cross-shaped RT-MS is designed for constructing a high-gain, high-aperture- efficiency, and CP-FP antenna. Through adjusting the off-center distances of the two metal-probes, respectively, a CP mode can be introduced. Then, the PCM having high reflectivity and LCPC property is applied for creating a FP antenna. This FP antenna was composed by the 9 × 9 cells arranged RT-MS array and coaxial-type patch source antenna. To further enhance the improvement of gain and bandwidth, an AMC structure surrounding the coaxial-type patch is utilized. The

proposed CP-FP antenna is fabricated and measured to validate the correctness of the design. The measurements demonstrated that the proposed antenna achieves high-gain and high aperture efficiency, and wider CP radiation property with a relative compact size, compared to other recent related works, which agree well with the simulated results. Because of the above better performance, the proposed antenna can be applied to many areas, such as RFID, WLAN systems, military communication, and so on.

REFERENCES

[1] K. Li, Y. Liu, Y. Jia, and Y. J. Guo, "A circularly polarized high-gain antenna with low RCS over a wideband using chessboard polarization conversion metasurfaces," *IEEE Trans. Antennas Propag.*, vol. 65, no. 8, pp. 4288–4292, Aug. 2017.

[2] Z. Wu, L. Li, Y. Li, and X. Chen, "Metasurface superstrate antenna with wideband circular polarization for satellite communication application," *IEEE Antennas Wireless Propag. Lett.*, vol. 10, pp. 907–910, 2015.

[3] Y. Huang, L. Yang, J. Li, Y. Wang, and G. Wen, "Polarization conversion of metasurface for the application of wide band low-profile circular polarization slot antenna," *Appl. Phys. Lett.*, vol. 109, no. 5, Aug. 2016, Art. no. 054101.

[4] H. L. Zhu, S. W. Cheung, K. L. Chung, and T. I. Yuk, "Linear-to-circular polarization conversion using metasurface," *IEEE Trans. Antennas Propag.*, vol. 61, no. 9, pp. 4615–4623, Sep. 2013.

[5] Z.-G. Liu, Z.-X. Cao, and L.-N. Wu, "Compact low-profile circularly polarized Fabry–Pérot resonator antenna fed by linearly microstrip patch," *IEEE Antennas Wireless Propag. Lett.*, vol. 15, pp. 524–527, 2016.

[6] Q. Chen and H. Zhang, "Dual-patch polarization conversion metasurface-based wideband circular polarization slot antenna," *IEEE Access*, vol. 6, pp. 74772–74777, 2018.

[7] Q. Chen and H. Zhang, "High-gain circularly polarized Fabry–Pérot patch array antenna with wideband low-radar-cross-section property," *IEEE Access*, vol. 7, pp. 8885–8889, 2019.

[8] P. Xie, G. Wang, H. Li, and J. Liang, "A dual-polarized two-dimensional beam-steering Fabry–Pérot cavity antenna with a reconfigurable partially reflecting surface," *IEEE Antennas Wireless Propag. Lett.*, vol. 16, pp. 2370–2374, 2017.

[9] C. Lin, Y. Ge, T. S. Bird, and K. Liu, "Circularly-polarized horns based on standard horns and a metasurface polarizer," *IEEE Antennas Wireless Propag. Lett.*, vol. 17, no. 3, pp. 480–484, Jan. 2018.

[10] B. A. Zeb and K. P. Esselle, "High-gain dual-band dual-polarised electromagnetic band gap resonator antenna with an all-dielectric superstructure," *IET Microw. Antennas Propag.*, vol. 9, no. 10, pp. 1059–1065, 2015.

[11] Y.-M. Cai, K. Li, W. Li, S. Gao, Y. Yin, L. Zhao, and W. Hu, "Dual-band circularly polarized transmitarray with single linearly polarized feed," *IEEE Trans. Antennas Propag.*, vol. 68, no. 6, pp. 5015–5020, Jun. 2020.

[12] Y. Cheng and Y. Dong, "Bandwidth enhanced circularly polarized Fabry–Pérot cavity antenna using metal strips," *IEEE Access*, vol. 8, pp. 60189–60198, 2020.

[13] F. Qin, S. Gao, G. Wei, Q. Luo, C. Mao, C. Gu, J. Xu, and J. Li, "Wideband circularly polarized Fabry–Pérot antenna [antenna applications corner]," *IEEE Antennas Propag. Mag.*, vol. 57, no. 5, pp. 127–135, Oct. 2015.

[14] N. Hussain, M.-J. Jeong, J. Park, and N. Kim, "A broadband circularly polarized Fabry–Pérot resonant antenna using a single-layered PRS for 5G MIMO applications," *IEEE Access*, vol. 7, pp. 42897–42907, 2019.

[15] N. Hussain, S. I. Naqvi, W. A. Awan, and T. T. Le, "A metasurface-based wideband bidirectional same sense circularly polarized antenna," *Int. J. RF Microw. Comput. Aided Eng.*, vol. 30, no. 8, 2020, Art. no. e22262.

[16] S. A. Muhammad, R. Sauleau, L. Le Coq, and H. Legay, "Self-generation of circular polarization using compact Fabry–Pérot cavity antennas," *IEEE Antennas Wireless Propag. Lett.*, vol. 10, pp. 907–910, 2011.

[17] Z.-G. Liu and W.-B. Lu, "Low-profile design of broadband high gain circularly polarized Fabry–Pérot resonator antenna and its array with linearly polarized feed," *IEEE Access*, vol. 5, pp. 7164–7172, 2017.

[18] L.-Y. Ji, P.-Y. Qin, Y. J. Guo, C. Ding, G. Fu, and S.-X. Gong, "A wideband polarization reconfigurable antenna with partially reflective surface," *IEEE Trans. Antenna Propag.*, vol. 64, no. 10, pp. 4534–4538, Oct. 2016.

[19] P. Naseri and S. V. Hum, "A dual-band dual-circularly polarized reflectarray for *K*/*Ka*-band space applications," in *Proc. 13th Eur. Conf. Antennas Propag. (EuCAP)*, Krakow, Poland, 2019, pp. 1–5.

[20] W. Chen, Z. Yu, J. Zhai, and J. Zhou, "Developing wideband dual-circularly polarized antenna with simple feeds using magnetoelectric dipoles," *IEEE Antennas Wireless Propag. Lett.*, vol. 19, no. 6, pp. 1037–1041, Jun. 2020.

[21] P. Xie, G. Wang, H. Li, J. Liang, and X. Gao, "Circularly polarized Fabry–Pérot antenna employing a receiver–transmitter polarization conversion metasurface," *IEEE Trans. Antennas Propag.*, vol. 68, no. 4, pp. 3213–3218, Apr. 2020.

[22] W. Pan, C. Huang, X. Ma, B. Jiang, and X. Luo, "A dual linearly polarized transmitarray element with 1-bit phase resolution in X-band," *IEEE Antennas Wireless Propag. Lett.*, vol. 14, pp. 167–170, 2015.

[23] A. Clemente, L. Dussopt, R. Sauleau, P. Potier, and P. Pouliguen, "1-bit reconfigurable unit cell based on PIN diodes for transmit-array applications in *X*-band," *IEEE Trans. Antennas Propag.*, vol. 60, no. 5, pp. 2260–2269, May 2012.

[24] D. J. Baena, B. S. Glybovski, P. J. del Risco, P. A. Slobozhanyuk, and A. P. Belov, "Broadband and thin linear-to-circular polarizers based on self-complementary zigzag metasurfaces," *IEEE Trans. Antennas Propag.*, vol. 59, no. 7, pp. 2513–2523, Jul. 2017.

[25] F. Diaby, A. Clemente, T. K. Pham, R. Sauleau, and L. Dussopt, "Circularly-polarized transmitarray antennas at ka-Band," *IEEE Antennas Wireless Propag. Lett.*, vol. 14, pp. 108–111, 2018.

[26] H. H. Tran and H. C. Park, "A simple design of polarization reconfigurable Fabry–Pérot resonator antenna," *IEEE Access*, vol. 8, pp. 91837–91842, 2020.

[27] Y. Wang and A. Zhang, "Dual circularly polarized Fabry–Pérot resonator antenna employing a polarization conversion metasurface," *IEEE Access*, vol. 9, pp. 44881–44887, 2021.

[28] Y. Ge and K. Qin, "Wideband high-gain circularly polarized Fabry–Pérot antenna feeding a conical short-horn," *Int. J. RF Microw. Comput. Aided Eng.*, vol. 28, no. 9, 2018, Art. no. e21430.

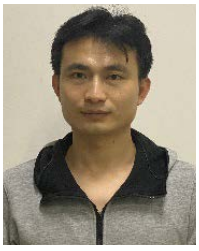

QIANG CHEN was born in Jiangxi, China. He received the master's and Ph.D. degrees from Air Force Engineering University (AFEU), Xi'an, China, in 2015 and 2019, respectively. He is currently a Lecturer with Air Force Early Warning Academy, Wuhan, Hubei, China. His research interests include microwave circuits, antennas, and arrays.

XIONG ZOU was born in Hubei, China, in 1987. He received the B.S. and Ph.D. degrees from Air Force Engineering University, Xi'an, China, in 2011 and 2015, respectively. He is currently with Early Warning Academy. He has authored or coauthored more than 30 papers in journals and conferences. His current research interests include microwave and millimeter-wave antennas and circuits and electronic countermeasures (ECM).

LIANG HONG was born in Wuhan, China. He received the B.S. and M.S. degrees from the Huazhong University of Science and Technology, Wuhan, in 2005 and 2011, respectively. His research interests include microwave devices and microwave technology.

DI ZHANG received the B.S., M.S., and Ph.D. degrees from Air Force Engineering University (AFEU), Xi'an, China, in 2013, 2015, and 2019, respectively. He is currently a Lecturer with Air Force Early Warning Academy. His research interests include RF orbital angular momentum antennas, reflect array antennas, and metasurface.

SIYU HUANG was born in Hunan, China. He received the B.S. degree from Hunan University, Changsha, China, in 2005, and the M.S. degree from Air Force Engineering University, Xi'an, China, in 2011. His research interests include microwave devices and microwave technology.

FANGLI YU was born in China, in 1983. He received the B.E. degree from Air Force Early Warning Academy, Wuhan, China. He is currently a lecture with Air Force Early Warning Academy, and also pursuing the Ph.D. degree with the School of Information and Engineering, Wuhan University of Technology. His current research interest includes radar signal processing.

WEIHUA XIONG was born in 1984. He received the master's degree from the Harbin Institute of Technology. He is currently a Lecturer at the Air Force Early Warning Institute. He has published more than ten technical papers, written three textbooks and monographs. He has three national invention patents. His research interests include electromagnetic field, microwave technology, antenna design, and radar detection.

HOU ZHANG received the B.S. degree in electromagnetic field and microwave technology from Xi'an Electronic and Engineering University, the M.S. degree in electromagnetic field and microwave technology from the Air force Missile College, and the Ph.D. degree in electromagnetic field and microwave technology from Xidian University. He has been the Session Chair of PIERS and APEMC. He has published over 150 technical papers and authored/edited six books. He is holding six granted/filed patents. His current research interests include planar antennas and EMC.